Desalination and Water Treatment
www.deswater.com
doi: 10.5004/dwt.2023.29344

286 (2023) 101–114
February

Magnetite/activated sludge hybrid process for the treatment of dye containing simulated textile wastewater

Behzat Balci*, Berika Ergan, F. Elçin Erkurt, Mesut Basibuyuk, Zeynep Zaimoglu, Fuat Budak, E. Su Turan

Cukurova University Department of Environmental Engineering, Balcali/Saricam, Adana 01136, Turkey, emails: behzatbalci@gmail.com (B. Balci), berikaergan@gmail.com (B. Ergan), eerkurt@cu.edu.tr (F. Elçin Erkurt), basibuyuk@cu.edu.tr (M. Basibuyuk), zeynepz@cu.edu.tr (Z. Zaimoglu), fbudak@cu.edu.tr (F. Budak), su.turan@gmail.com (E. Su Turan)

Received 22 September 2022; Accepted 31 January 2023

ABSTRACT

Addition of a magnetically separable magnetite as an adsorbent to the activated sludge (AS) process can provide significant advantages in the treatment of dye-containing textile wastewater. This study investigated the potential of magnetite/activated sludge (M/AS) as an adsorption/biodegradation hybrid process to treat Reactive Red 195 (RR195) containing simulated textile wastewater. RR195 and chemical oxygen demand (COD) removal studies were performed separately with magnetite, activated sludge, and M/AS hybrid processes. The Freundlich isotherm was determined to be the best model with (R^2 = 0.999) to describe the adsorption of the RR195 onto magnetite. Different concentrations of mixed liquor suspended solids (MLSS) of the activated sludge process and the magnetite were used simultaneously in the M/AS hybrid process. The M/AS hybrid process experiments showed that the RR195 removal efficiency increased with increasing MLSS and the magnetite concentrations. 4,000 mg/L was determined as the optimum MLSS concentration to remove the RR195 from simulated textile wastewater by the M/AS hybrid process. While the RR195 removal efficiency was 76.10% by activated sludge containing 4,000 mg/L MLSS in 90 min, the RR195 removal efficiency increased to 99.5% with the simultaneous use of 2.5 g/L magnetite and activated sludge containing 4,000 mg/L MLSS. The COD removal efficiency was determined as 94.32% by simultaneous using activated sludge containing 4,000 mg/L MLSS and 5 g/L magnetite. The magnetite particles can be separated from simulated textile wastewater and activated sludge biomass after M/AS hybrid process treatment by applying a magnetic field. The results of the study have shown that the M/AS hybrid system is an effective process for the treatment of dye-containing textile wastewater.

Keyword: Activated sludge; Adsorption; Magnetite; Hybrid process; Textile dye

1. Introduction

The textile industry is one of the important industries threatening surface water resources worldwide as it produces wastewater containing high amounts of salts, auxiliary chemicals and synthetic dyes [1]. The most important pollutants in textile wastewater are synthetic dyes. Approximately 70% of the dyes used in the textile industry are azoic dyes. Azoic dyes are aromatic compounds with one or more –N=N– groups [2–5]. Discharge of wastewater containing textile dyes into aquatic environments may cause aesthetic problems, deterioration of photosynthesis activities, reduction of gas transfers and toxic effects on aquatic organisms [6–9]. Therefore, it is vital to treat wastewater containing dyes with appropriate methods before they are discharged into aquatic environments. Several methods are used to treat the

* Corresponding author.

dye-containing textile wastewaters, such as physical, chemical, biological or combination of different processes [10–13].

Biological wastewater treatment processes based on biodegradation and biosorption are known as eco-friendly and cost-effective methods [14]. The azoic dyes are generally stable to the aerobic biodegradation [4]. On the other hand, cleavage of the azo bonds occurs in an anaerobic/anoxic biological process due to transferring the electrons from nicotinamide adenine dinucleotide hydrogen (NADH) to azo bonds [15]. However, colorless aromatic amines are formed as a result of the degradation of azo bonds under the anaerobic/anoxic process. Aromatic amines can be strongly carcinogenic and mutagenic to humans, animals, and plants [16]. In addition, some types of aromatic amines can be more cyto- and genotoxic than the original form of azo dyes. Aromatic amines are strongly resistant to anaerobic degradation. Therefore, an aerobic process is required after anaerobic treatment to remove the aromatic amines from textile wastewater [4]. Hence, the commonly used biological method for treating azo dye-containing textile effluents is sequencing the anaerobic and aerobic process [17,18]. The fate of the aromatic amines in the aerobic processes varies according to the chemical structures of the aromatic amines. Removal efficiencies of different aromatic amines by aerobic process range from 37% to 100% [4,16,19,20]. Additionally, aromatic amines can inhibit the degradation potential of the aerobic biomass due to their toxic effects [21]. Some types of aromatic amines can be accumulated in the aerobic sludge. Land application for the disposal of aerobic sludge containing aromatic amines poses a potential risk to soil ecosystems [4,22] Treatment of azo dye containing textile wastewater by the sequencing anaerobic/aerobic system also poses a risk to environmental health due to residual aromatic amines in the textile effluents and aerobic sludge. On the other hand, biodegradable compounds which cause high chemical oxygen demand (COD) can be removed from textile wastewater by aerobic biological processes. While aerobic processes have a great potential to remove biodegradable compounds, different processes are required for the removal of dyes from textile wastewater. The adsorption process stands out among other processes due to its easy application in dye removal from textile wastewater and providing high-quality effluent [23]. However, the adsorption process alone is not sufficient to remove organic pollutants other than dyes from textile wastewater. Therefore, it is a suitable method to use the adsorption process together with additional processes in the treatment of textile wastewater. The sequential use of an adsorption process and an aerobic biological process in the treatment of textile wastewater can provide high quality effluent. However, the operation of two separate reactors in sequential processes causes increase in plant costs. In addition, these systems require high contact times to treat wastewater. The integrated use of adsorption and aerobic biological processes in a single reactor can provide advantages such as protection of the biological system from toxic effects, synergistic pollutant removal, treatment of wastewater in a shorter time, and lower investment and operating costs [24,25]. In addition, the industries with an aerobic biological system can be quickly and easily converted to the adsorption/aerobic biological integration process. Activated carbon in powder form (PAC) can be added to aerobic processes to enhance the removal of recalcitrant pollutants such as textile dyes. PAC can be added directly to the aeration tank or the sludge recycle line of the biological treatment. The addition of the PAC to the activated sludge (AS) process is known as the powdered activated carbon treatment process (PACT) [26]. The residence time of the activated carbon in the system is related to the sludge retention time (SRT). However, PAC cannot be separated from the AS before the sludge dewatering and digestion processes. Thus, the addition of the PAC to the AS increases the solid load of sludge dewatering and digestion processes. Also, PAC decreases the methane production in the sludge digester due to its inorganic form. Therefore, separating the adsorbent from biological sludge in an integrated system is a vital step. The investigation of iron oxide particles in the removal of pollutants from wastewater by adsorption has become quite common in recent years [27–30] magnetite (Fe_3O_4) stands out among the other iron oxide particles due to its unique properties such as large specific surface area, high magnetic saturation, and non-toxicity [31]. Also, magnetite nanoparticles have Fe^{+3} and Fe^{+2} cations in their crystal structure [32]. Magnetite nanoparticles can be easily separated from the bulk solution after the adsorption process by applying an external magnetic field [33]. The integrated application of the activated sludge process with an adsorbent that can be separated from a liquid–solid mixture such as magnetite should be investigated for its potential in textile wastewater treatment. There is currently no study on this subject in the literature.

This study aims to investigate the potential of the magnetite/activated sludge (M/AS) hybrid process for the treatment of simulated textile wastewater containing Reactive Red 195 (RR195) and production auxiliary chemicals. The magnetite can be separated from M/AS process after treatment.

Studies on dye removal in the literature are generally not on the integration of an adsorbent with a biological process, but on the use of these processes separately. It is thought that the lack of the research on integrated adsorption/biological process in literature is due to separation problem of the adsorbent from the AS. On the other hand, the current studies based on dye removal by magnetite and magnetite-based composite adsorbents were carried out with deionized water containing only dye molecules [34–36]. Also, biosorption-based dye removal studies with AS have generally been carried out with aqueous solutions that do not contain textile chemicals other than the dye molecules [37,38]. These studies reveal the specific interactions of an adsorbent and dye molecules with various mathematical expressions. However, textile production is a complex process consisting of many stages. In these stages, different types of chemicals are used for fiber production and these chemicals are transferred to the textile wastewater [39,40]. Presence of various auxiliary chemicals in wastewater can affect the dye removal capacities of the adsorbents due to competitive sorption between dye molecules and auxiliary chemicals. In this study, a realistic simulated textile wastewater containing textile production auxiliary chemicals was used. It is thought that the data obtained from this study can make important contributions to the literature.

2. Material and methods

2.1. Production of magnetite

Magnetite was synthesized using the co-precipitation method under alkaline conditions. All chemicals used for the magnetite production were of analytical purity degree. $FeCl_3 \cdot 6H_2O$ (Merck, CAS: 10025-77-1, >99%) and $FeSO_4 \cdot 7H_2O$ (Merck, CAS: 7782-63-0, >99%) were used to produce the magnetite particles. The stoichiometric molar ratio of Fe^{3+}:Fe^{2+} for magnetite formation is 2:1 [41]. 9.2 g $FeCl_3 \cdot 6H_2O$ and 5.0 g $FeSO_4 \cdot 7H_2O$ were dissolved in 200 mL distilled water. 0.5 mL Oleic Acid ($C_{18}H_{34}O_2$, Merck, CAS: 112-80-1, >99%) was added to the mixture as a surface stabilizer. Finally, 20 mL NH_4OH (Supelco, CAS: 1336-21-6, 25%) solution was added dropwise to the formation of black iron oxide precipitate and the mixture was stirred at 80°C within 2 h under nitrogen atmosphere. The mixture was centrifuged and the solid phase was washed with distilled water and ethanol. The product was dried at 60°C for 24 h and stored in a nitrogen atmosphere.

2.2. Characterization of magnetite

The morphological investigation and the elemental analysis of the magnetite were performed by scanning electron microscopy (SEM), energy-dispersive X-ray spectroscopy (EDX) (FEI Quanta 650 Field Emission), respectively. The Brunauer–Emmett–Teller (BET) method was used to determine the specific surface area of the magnetite (Quantachrome, Sorptometer 1042). The magnetic properties of the magnetite were determined by a superconducting quantum interference device magnetometer (Quantum Design, PPMS DynaCool-9). The associated functional groups of the magnetite were investigated by Fourier-transform infrared spectroscopy (FTIR) (Jasco, FT/IR-6700). The crystalline phases of the magnetite were identified by X-ray diffraction (XRD) in the 2θ scan range of 10°–90° (PANalytical EMPYREAN XRD).

2.3. Composition of the simulated textile wastewater

A local textile industry was used as the basis to determine the content of simulated textile wastewater (STW). The auxiliary chemicals concentrations in the STW were determined by considering the usage dosage in the production stages and the dilution factor from production to wastewater generation in the facility. Also, inorganic nutrients and trace elements were added to the STW for the growth of activated sludge biomass [42]. The composition of the STW is given in Table 1.

Table 1
Composition of the simulated textile wastewater

Production chemical	Description	Concentration
Reactive Red 195	Dye	100 mg/L
Modified starch	Sizing chemical	1,000 mg/L
Acetic acid	pH adjuster	0.10 ml/L
10% NaOH	Mercerization	0.60 ml/L
H_2O_2	Bleacher	0.18 ml/L
Stabilol ZM	Stabilizer	0.60 ml/L
Cottonclarin TR	Wetting chemical	0.40 ml/L
Sera Wet CAS	Rapid wetting chemical	0.20 ml/L
Perlavin SRD	Soaping chemical	0.50 ml/L
Locanite CNT	Washing chemical	60 mg/L
Securon 1420	Ion trap	0.20 ml/L
Seragal MIP-O_2	Dyeing chemical	125 mg/L
NaCl	Dyeing promoter	3,000 mg/L
$NaHCO_3$	Dyeing promoter, pH adjuster	1,500 mg/L
Colorfix NF2P	Dye fixer	50 mg/L
Setasil KF-1920	Softener	50 mg/L
Belsoft 200	Softener	50 mg/L
Tubingal MAC	Sanforizing chemical	125 mg/L
Chemical oxygen demand		1,945–2,320 mg·O_2/L
pH		7.81

Inorganic nutrients (mg/L)		Trace elements (μ/L)			
NH_4Cl	25	H_3BO_3	50	$(NH_4)_6Mo_7O_{24} \cdot 4H_2O$	50
K_2HPO_4	20	$ZnCl_2$	50	$AlCl_3$	50
$CaCl_2$	20	$CuCl_2$	30	$CoCl_2 \cdot 6H_2O$	50
$MgSO_4$	15	$MnSO_4 \cdot H_2O$	50	$NiCl_2$	50
$FeSO_4 \cdot 7H_2O$	15				

2.4. Analytical methods

The RR195 concentration analysis was performed with a calibration curve prepared at a wavelength of 541 nm in a spectrophotometer (35 UV/VIS-Perkin Elmer). The COD analysis was carried out with the closed reflux titrimetric method [43]. All analyzes were carried out by approved methods.

2.5. Dye removal experiments

2.5.1. Adsorption of the RR195 from STW by magnetite

RR195 removal experiments were conducted with magnetite and M/AS separately. Batch adsorption experiments were carried out to remove RR195 from STW by magnetite. The experiments were performed with 200 mL STW and 100 mg/L RR195. Eight different magnetite concentrations were investigated (0.312, 0.625, 1.25, 2.5, 3.75, 5.0, 7.5, and 10 g/L) on the adsorption of RR195 from STW. The samples were withdrawn at certain time intervals, centrifuged for 10 min at 4,000 rpm and the supernatant was used for the measurement of the dye concentration. The data obtained from the adsorption experiments were applied to different adsorption isotherms. The amount of the RR195 adsorbed by the adsorbent at different times (q_t) was calculated from Eq. (1). All experiments were performed at pH 7 and 20°C.

$$q_t = \frac{\left(C_0 - C_t\right)V}{m} \tag{1}$$

where C_0 = initial RR195 concentration, mg/L; C_t = residual RR195 concentration at certain time (t), mg/L; V = volume of the solution, L; m = amount of the magnetite, g.

2.5.2. RR195 removal studies from STW by M/AS

The activated sludge process was acclimated to STW before the M/AS experiments. RR195 was not added to STW in the adaptation process to prevent the adsorption of the dye molecules by activated sludge biomass. The acclimation of the activated sludge to STW was performed by sequencing batch reactor (SBR) process. The acclimation process was carried out with 3,000 mg/L mixed liquor suspended solids (MLSS), 24 h hydraulic retention time (HRT) and 15 d solid retention time (SRT) in an 8-L cylindrical tank. The oxygen was supplied by air diffusers. At the same time, the reactor contents were mixed with the supplied air. The adaptation phase was continued until a stable COD value was obtained in the effluent. The RR195 removal studies by M/AS were carried out in 500 mL flasks, including 200 mL STW containing 100 mg/L RR195. The mixing and aeration of M/AS was conducted by orbital shaking at 300 rpm. The RR195 removal studies were performed with three MLSS concentrations (2,000; 3,000 and 4,000 mg/L). Also, five magnetite concentrations (0.312, 0.625, 1.25, 2.50, and 3.75 g/L) were used for each MLSS concentration. Five RR195 concentrations (50, 100, 150, 200, and 300 mg/L) were studied with the addition of different amounts of magnetite into activated sludge, including 4,000 mg/L MLSS. Also, the COD removal studies were carried out with three different MLSS concentrations (2,000; 3,000 and 4,000 mg/L) and five magnetite concentrations (1.25, 2.50, 3.75, and 5.0 g/L). The samples were withdrawn at certain time intervals and centrifuged at 3,000 rpm and the supernatant was analyzed. Active and inactive biomass were used for the RR195 removal from STW to understand whether the dye degraded. The inactivation of the biomass was carried out by immersing the biomass in a 5.0 g/L sodium azide (NaN_3) solution for 24 h [44]. All M/AS experiments were conducted at 20°C and pH 7.0.

2.5.3. Statistical analysis

The statistical analysis of the data obtained from the experiments was performed by SPSS Statistics 21.0 with 95% ($p \leq 0.05$) confidence interval. All adsorption and M/AS experiments.

2.6. Adsorption isotherms and their validation methods

Applying adsorption data to different isotherm models is an important step to understand the adsorption mechanism. Adsorption isotherms help to understand the distribution of adsorbate molecules to the surface of an adsorbent at equilibrium time. Also, some isotherm models allow predicting the maximum adsorption capacity of the adsorbent for adsorbate at equilibrium time [45,46]. The adsorption data were applied to several isotherm models (Langmuir, Freundlich, Dubinin–Radushkevich, Sips, Toth, Jovanovich, and Redlich–Peterson isotherms). Information about the maximum adsorption capacity of magnetite and the distribution of RR195 molecules on the magnetite surface can be obtained by applying the data obtained from the adsorption experimental process to these isotherm models. The non-linear equations and the descriptions of the adsorption isotherms are given in Table 2. Non-linear regression analysis was used to obtain the isotherm parameters. The nonlinear regression method allows using the original form of the isotherm equation to estimate isotherm parameters [47,48]. Eight data points from the different amounts of magnetite were used for the non-linear regression analysis of adoption isotherm parameters. The coefficient of determination (R^2) [Eq. (2)], sum square error (ERRSQ) [Eq. (3)], Average Percentage Errors (APE %) [Eq. (4)], Chi-square test (χ^2) [Eq. (5)], hybrid fractional error function (HYBRID) [Eq. (6)] and Marquardt's percent standard deviation (MPSD) [Eq. (7)] error functions, indicate the difference between the experimental data and the calculated values, and these were taken into account to determine the performance of the data-fitting isotherm model. The best-fit isotherm selection was made according to the high value of the R^2 coefficient and low values of ERRSQ, APE %, χ^2, HYBRID and MPSD [49].

$$R^2 = \frac{\left(q_{e,\exp} - \overline{q_{e,\text{cal}}}\right)^2}{\sum\left(q_{e,\exp} - \overline{q_{e,\text{cal}}}\right)^2 + \left(q_{e,\exp} - q_{e,\text{cal}}\right)^2} \tag{2}$$

$$\text{ERRSQ} = \sum_{i=1}^{N}\left(q_{e,\text{cal}} - q_{w,\exp}\right)^2 \tag{3}$$

$$\text{APE\%} = \frac{\sum_{i=1}^{N}\left|\left(q_{e,\exp} - q_{e,\text{cal}}\right)/Q_{e,\exp}\right|}{N} \times 100 \tag{4}$$

Table 2
Applied adsorption isotherms

Isotherm	Non-linear equation	Description
Langmuir	$q_e = \frac{q_{\max} K_L C_e}{1 + K_L C_e}$	Langmuir isotherm model describes monolayer surface adsorption. Adsorption and desorption of the adsorbate rates are relatively balanced in equilibrium [51]. q_e is the adsorption capacity (mg/g) at the equilibrium, C_e is the adsorbate concentration in solution at the equilibrium time (mg/L), $q_{\max}$ is the maximum adsorption capacity (mg/g), and K_L is the isotherm constant (L/mg) [Eq. (8)].
Freundlich	$q_e = K_F C_e^{1/n}$	Freundlich isotherm describes the adsorption of molecules onto heterogeneous surfaces. K_F is the isotherm constant related to the adsorption capacity (L/mg) and "n" indicates the energy distribution and the intensity of the surface [Eq. (9)]. A value of "n" greater than 1 indicates that adsorption is favorable [50,52].
Dubinin–Radushkevich	$q_e = q_{\max} \exp\left(-b_D \varepsilon^2\right)$ $\varepsilon = RT \ln\left(1 + \frac{1}{C_e}\right)$	The D-R isotherm model describes the adsorption mechanism onto heterogeneous surfaces by calculating the Gaussian energy distribution of adsorbate [53]. b_D (mol²/kJ²) is the Dubinin–Radushkevich isotherm constant, and ε is the Polanyi potential [Eqs. (10) and (11)] [54].
Sips	$q_e = \frac{q_{\max} K_S C_e^{1/n_S}}{1 + K_S C_e^{1/n_S}}$	The Sips isotherm is derived from the Langmuir and Freundlich isotherms, and it describes the adsorption mechanism on heterogeneous surfaces. K_S is the constant of the model and n_S is the model exponent [Eq. (12)] [55].
Toth	$q_e = \frac{q_{\max} K_T C_e}{\left[1 + \left(K_T C_e\right)^{n_T}\right]^{1/n_T}}$	The Toth model was obtained by empirical modification of the Langmuir isotherm. This isotherm is quite successful in describing the adsorption of adsorbate on heterogeneous surfaces at high and low concentrations. K_T is the isotherm constant (L/mg) and "n_T" characterizes the surface heterogeneity [Eq. (13)]. If the "n_T" value is 1, the equation is reduced to the Langmuir model [56,57].
Jovanovich	$q_e = q_{\max}\left[1 - \exp\left(-K_J C_e\right)\right]$	The Jovanovich isotherm [Eq. (14)] was obtained by modifying the Langmuir isotherm by adding adsorbent and adsorbate mechanical interactions. The model is successful in describing the monolayer adsorption processes. The model approaches Henry's Law at low adsorbate concentrations. K_J (L/mg) is Jovanovich constant [55,58].
Redlich–Peterson	$q_e = \frac{K_r C_e}{1 + a_r C_e^{\beta}}$	The Redlich–Peterson equation is an empirical hybrid isotherm of the Freundlich and Langmuir isotherms. The model can describe the adsorption phenomena on homogeneous and heterogeneous surfaces. K_r (L/g) and a_r (L/mg) are the constants of the model. β is the exponent of the model and ranges between 0–1 [Eq. (14)]. When β close 1, the model close to the Langmuir model, if β = 0, the model leans towards the Freundlich model [59].

$$X^2 = \sum_{i=1}^{N} \frac{\left(q_{e,\text{cal}} - q_{e,\text{exp}}\right)^2}{q_{e,\text{exp}}} \tag{5}$$

$$\text{HYBRID} = \frac{100}{N-P} \sum_{i=1}^{N} \left[\frac{\left(q_{e,\text{exp}} - q_{e,\text{cal}}\right)^2}{q_{e,\text{exp}}} \right] \tag{6}$$

$$\text{MPSD} = \sqrt{\frac{1}{N-P} \sum_{i=1}^{N} \left(\frac{\left(q_{e,\text{exp}} - q_{e,\text{cal}}\right)}{q_{e,\text{exp}}} \right)^2} \tag{7}$$

where $q_{e,\text{exp}}$ is the amount of the dye molecules adsorbed per unit mass of magnetite (mg/g) at equilibrium time, $q_{e,\text{cal}}$ is the amount of the dye molecules adsorbed per unit mass of magnetite (mg/g) at equilibrium time predicted by isotherm model, N is the number of experimental data, and P is the number of the isotherm parameters [50].

3. Results and discussion

3.1. Characterization of the magnetite

3.1.1. Morphological and elemental analysis of the magnetite

The morphological and elemental analysis of the magnetite was carried out by SEM and EDX analyses, respectively (Fig. 1). The SEM analysis of the magnetite (400,000x) showed that the magnetite particles have cubic structure and different congregate structures. magnetite particles tend to agglomerate due to their high surface energies and attractive

dipole forces [60]. The obtained results from the EDX analysis confirmed the presence of iron and oxygen elements. The weight percent of the iron and the oxygen element of magnetite were determined as 63.93% and 23.96%, respectively. The signal of the carbon element (12.11%) corresponds to oleic acid, which was used as a surface stabilizer.

3.1.2. BET analysis of the magnetite

The performance of an adsorbent in wastewater treatment applications increases with increasing surface area of the adsorbent. Generally, the agglomeration of magnetite particles can cause decrease in the specific surface area. Surface stabilizers such as oleic acid can partially prevent surface area reduction due to agglomeration [61,62]. The specific surface area, total pore area, and total pore volume of the magnetite were determined as 55.873 m^2/g, 5.010 m^2/g, and 0.210 cm^3/g, respectively by the BET analysis (Fig. 2). The BET isotherm curve of the magnetite displays Type IV isotherm. Type IV isotherm is generally related to uniform mesoporous structure adsorbents [63].

3.1.3. XRD pattern of the magnetite

The crystalline nature of the magnetite investigation was carried out by the XRD technique in the 2θ scan range of 10°–90° (Fig. 3). The XRD pattern matched well in peak position and intensity of the magnetite pattern (Card No: 98-015-8741). The crystalline nature of magnetite is a cubic spinel structure [64]. The XRD analysis of the magnetite showed sharp and intensive peaks corresponding to cubic spinel crystal structure. The XRD analysis confirmed that the produced adsorbent was magnetite.

3.1.4. FTIR analysis

The FTIR analysis was carried out to investigate the associated functional groups of the magnetite (Fig. 4). In the FTIR analysis of the magnetite, the wide peak that appeared at 3,427 cm^{-1} can be related to –OH stretching vibration due to adsorption of water molecules onto the magnetite surface [63,65]. The peak which appeared at 557 cm^{-1} denotes the presence of Fe–O bonds stretching [63,66]. The peak detected at 2,950 cm^{-1} is related to stretching modes of CH_2 from oleic acid [63]. The peak at 1,032 cm^{-1} belongs to CH_3 bending from oleic acid. The signal that appeared at 1,616 cm^{-1} is related to carboxylate (COO^-) stretching from oleic acid [67]. The presence of the CH_2, CH_3 and COO^- showed that the surface of the magnetite was coated by oleic acid.

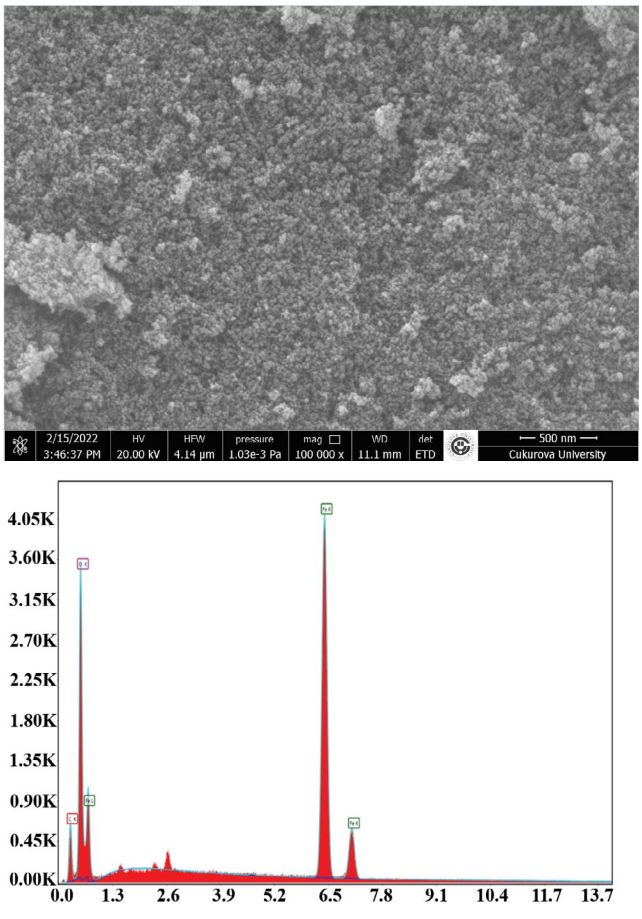

Fig. 1. Scanning electron microscopy and energy-dispersive X-ray spectroscopy analyses of the magnetite.

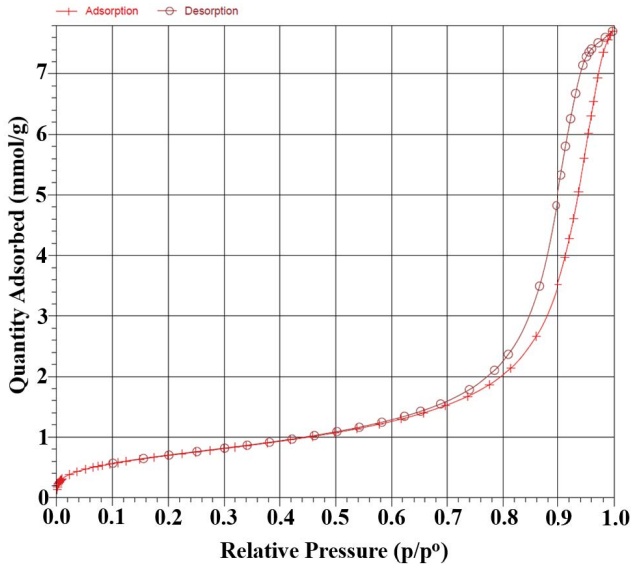

Fig. 2. Brunauer–Emmett–Teller analysis of the magnetite.

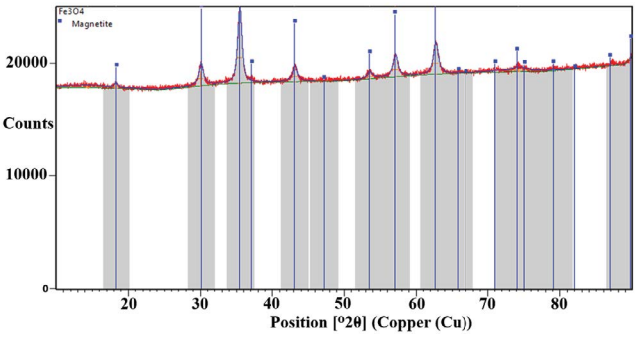

Fig. 3. X-ray diffraction analysis of the magnetite.

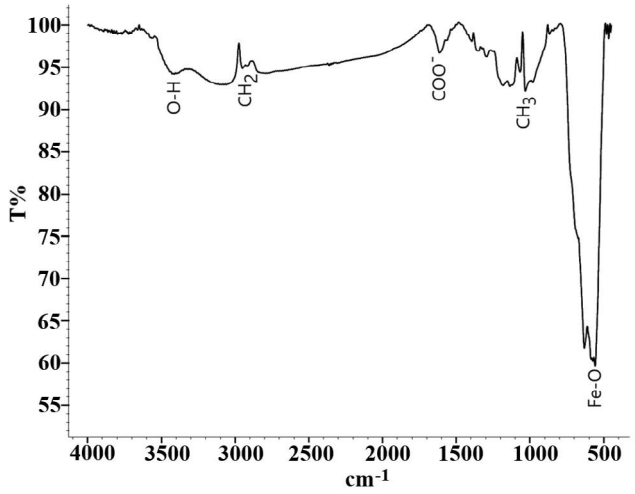

Fig. 4. Fourier-transform infrared spectroscopy analysis of the magnetite.

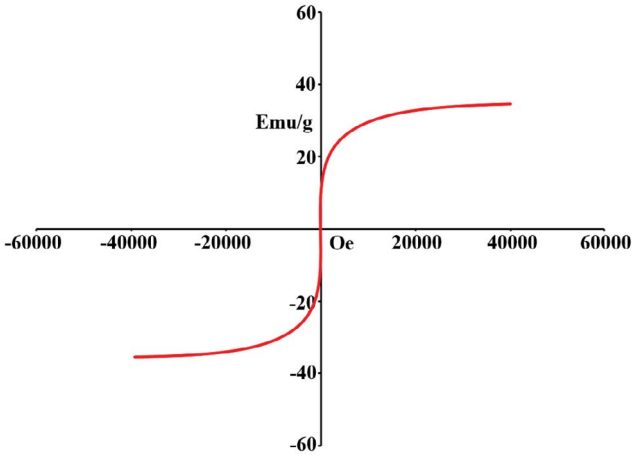

Fig. 5. Magnetic specification of the magnetite.

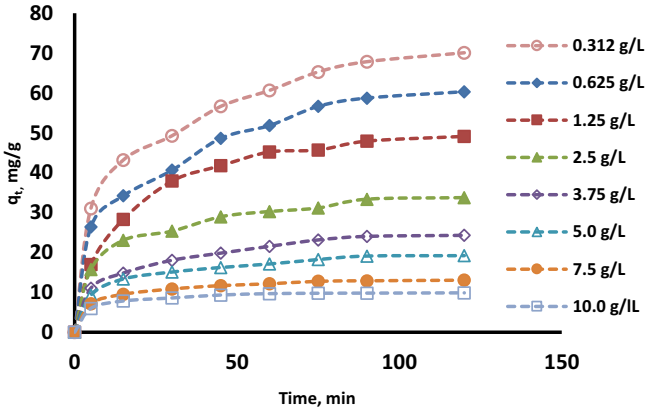

Fig. 6. Adsorption of the Reactive Red 195 by different concentrations of magnetite.

3.1.5. Magnetic specifications of the magnetite

Magnetization value of magnetite particles is an important parameter which shows the efficiency of separating the adsorbent from the liquid phase. Generally, magnetic saturation values of superparamagnetic iron oxide particles range from 30 to 50 emu/g. The particle size distribution, spaces between the particles and the crystalline structure of iron oxide affect the magnetic properties [68]. The magnetic curve of magnetite showed superparamagnetic behavior (Fig. 5) [63]. The saturation magnetization value of the magnetite was determined as 35.72 emu/g.

3.2. Adsorption of RR195 from STW by the magnetite

The adsorption of 100 mg/L RR195 was performed with the magnetite concentrations ranging between 0.312–10.0 g/L at pH 7 and 20°C (Fig. 6). Determination of the equilibrium time is an essential step for the adsorption experiments. Accurately determining equilibrium time dramatically contributes to the design of real-scale adsorption processes. It is necessary to determine the "q_e" value, which is the amount of solute (mg) adsorbed in the unit weight (g) of the adsorbent at the equilibrium time. However, it is difficult to determine the real "q_e" value due to the slow interaction between adsorbate and adsorbent after the initial rapid reaction in many adsorption processes. In such cases, the closest "q_e" value is selected [69]. The equilibrium times for 0.312, 0.625, 1.25, and 2.5 g/L of magnetite was determined as 75 min. On the other hand, the equilibrium times for 3.75, 5.0, 7.5, and 10.0 g/L of magnetite were determined as 30 min. The adsorption of RR195 by magnetite at concentrations above 2.5 g/L was rapid within the first 15 min, then became slow with increasing contact time due to high binding sites of magnetite per RR195 molecules. High sorption sites per RR195 molecules may cause rapid diffusion intraparticle matrix of magnetite [70]. The adsorption capacities at equilibrium time for 0.312, 2.5, and 10.0 g/L magnetite concentrations were calculated as 65.28, 31.16 and 9.77 mg/g, respectively. RR195 removal efficiencies from STW at equilibrium time for 0.312, 2.5, and 10.0 g/L magnetite concentrations were found to be 20.4%, 77.9% and 97.78%, respectively. As the adsorbent dosage increases, the number of the adsorbing active sites per unit solution volume increases. The presence of more actives site can increase the dye removal efficiency [71]. Determining the effective adsorbent dose is very important to achieve the desired dye removal efficiencies in real-scale applications. On the other hand, the effective adsorbent dose is directly related to the dye concentration in the wastewater. With the increase of the dye concentration in the wastewater, the required effective dose of adsorbent increases [72].

3.2.1. Adsorption isotherms

The calculated adsorption isotherm parameters are shown in Table 3. The highest maximum adsorption capacity (93.197 mg/g) of the magnetite for the RR195 was obtained from the Langmuir isotherm with a moderately high R^2 (0.985) value among the tested isotherms. However, high ERRSQ (63.146) and HYBRID (68.777) function values for the Langmuir isotherm showed that this isotherm is not appropriate for the description of the experimental data. The R^2 value is not sufficient for selecting the isotherm in

Table 3
Calculated isotherm parameters

Isotherm	Constants	Error functions					
Langmuir		R^2	ERRSQ	APE %	χ^2	HYBRID	MPSD
q_{max}	93.197	0.985	63.146	13.493	4.126	68.777	0.241
K_L	2.351						
Freundlich							
K_F	5.541	0.999	2.76	2.54	0.417	2.08	0.0485
n	1.785						
Dubinin–Radushkevich							
q_{max}	69.774	0.932	294.6	29.472	18.941	315.695	1.508
K_{DR}	0.007						
Redlich–Peterson							
K_r	132.695	0.998	3.015	1.573	0.435	2.37	0.411
a_r	23.348						
β	0.443						
Toth							
q_{max}	65.241	0.990	40.014	11.216	2.999	59.997	1.230
K_T	28.755						
n_T	1.045						
Jovanovich							
q_{max}	68.998	0.986	75.281	14.880	4.443	25.813	1.62
K_J	0.028						
Sips							
q_{max}	61.215	0.934	224.016	19.832	8.86	177.234	2.82
K_S	0.021						
n_S	0.727						

the non-linear solution method. Along with high R^2 values, high error function values can also be obtained from the non-linear method [73]. The lowest R^2 and the highest APE %, ERRSQ and HYBRID values were calculated for the Dubinin–Radushkevich isotherm. The Dubinin–Radushkevich model was found to be insufficient for describing the adsorption of the RR195 onto magnetite. The error function values of the Sips isotherm showed similarities with the Dubinin–Radushkevich isotherm. The Jovanovich model predicted the maximum adsorption capacity as 68.998 mg/g, closer to the maximum experimental q_e (65.28 mg/g) value with moderate error function values. It can be seen from Table 2 that the adsorption data fitted well to the Freundlich and Redlich–Peterson isotherms. Among the tested isotherms, the highest R^2 value (0.999), lowest ERRSQ (2.76), χ^2 (0.417), HYBRID (2.08) and MPSD (0.0485) values were obtained from the Freundlich isotherm. The adsorption data fitted to the Freundlich isotherm perfectly. When considering the assumption of the Freundlich isotherm, it is thought that the sorption sites of the magnetite are heterogeneous and have different adsorption energies. The RR195 molecules distributed non-uniformly to the sorption sites and were adsorbed onto magnetite surface with multilayers. The "n" value was calculated as 1.785, indicating that the adsorption process is favorable [50,74].

3.3. RR195 removal from STW by M/AS process

100 mg/L RR195 removal studies from STW by the M/AS process were carried out simultaneously using three different MLSS concentrations (2,000; 3,000 and 4,000 mg/L) with five different magnetite concentrations (0.312, 0.625, 1.25, 2.50, and 3.75 g/L). Also, removal of five different RR195 concentrations (50, 100, 150, 200, and 300 mg/L) by 4,000 mg/L MLSS with different amounts of magnetite were studied. The percentage of volatile suspended solids of MLSS was determined between 84% and 87%. A stable COD effluent was obtained after approximately 28 d in the adaptation phase of the activated sludge process to the dye-free simulated textile wastewater. Acclimated activated sludge was operated for another 10 d. The M/AS process was carried out by preparing the desired MLSS concentrations from the acclimated AS.

3.3.1. Effect of MLSS and magnetite concentrations for the removal of RR195

The M/AS hybrid experiments were performed with 100 mg/L RR195 concentration (Fig. 7). The difference between the RR195 removal efficiencies by inactivated biomass (sodium azide, 5 g/L) and the activated biomass

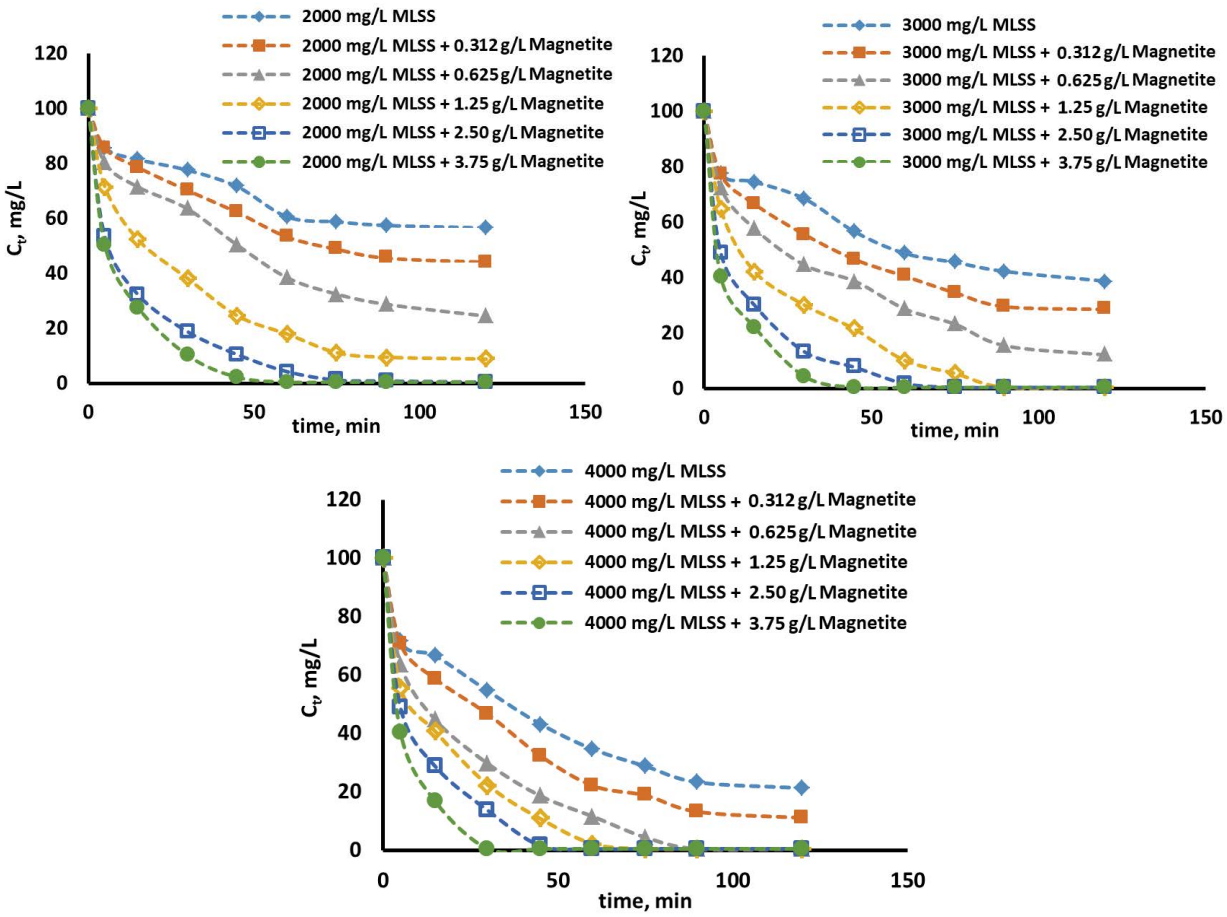

Fig. 7. Effect of mixed liquor suspended solids and magnetite concentrations on the removal of Reactive Red 195 by magnetite/activated sludge.

was negligible. The mechanism of the RR195 removal with biomass is thought to be adsorption, with no biodegradation. The results of the study showed that the MLSS concentration has a significant effect on the removal of RR195. It was determined that the RR195 removal efficiency increases with increasing MLSS concentration. The RR195 removal efficiencies within 90 min for 2,000; 3,000 and 4,000 mg/L MLSS without magnetite were determined as 42.5%, 57.7% and 76.1%, respectively. Many studies reported that the biosorption of Reactive textile dyes onto activated sludge increases by decreasing the pH of the medium [75–77]. Carboxyl, phosphate, and amine ionized groups make the surface charge of the activated sludge biomass negative. Reactive dyes are negatively charged due to their sulfonated groups. Therefore, electrostatic repulsive forces between reactive dyes and active biomass may adversely affect the biosorption process. When the pH value of the solution is adjusted to below the isoelectric point of the cell's surface charge, the charge of the activated sludge becomes positive as a result of the amine groups protonation [78]. Positively charged amine groups are responsible for the adsorption of reactive dyes [79]. However, acidification of the textile wastewater is not possible for the activated sludge systems due to the inhibition of the microorganisms. The M/AS experiments showed that the magnetite concentration has a significant effect on the removal of the RR195 from STW. The RR195 removal efficiencies within 60 min with the simultaneous use of 0.312, 1.25, and 3.75 g/L magnetite concentrations with 2,000 mg/L MLSS were found to be 46.70%, 82.20%, and 99.50%, respectively. The experiments showed that at least 1.25 g/L magnetite concentration was necessary to achieve more than 90% dye removal within 90 min for the activated sludge process containing 2,000 mg/L MLSS. On the other hand, ~90% RR195 removal efficiency can be obtained within 30 min by adding magnetite with 3.75 g/L concentration into the activated sludge process containing 2,000 mg/L MLSS. The RR195 removal efficiencies within 60 min for 0.312 g/L magnetite/3,000 mg/L MLSS-AS, 2.50 g/L magnetite/3,000 mg/L MLSS-AS, and 3.75 g/L magnetite/3,000 mg/L MLSS-AS were found to be 59.4%, 89.20%, and 99.50%, respectively. 99.50% RR195 removal efficiency was obtained in 90 min by 1.25 g/L magnetite/3,000 mg/L MLSS-AS. On the other hand, this efficiency was achieved in 45 min by 3.75 g/L magnetite/3,000 mg/L MLSS-AS. The highest RR195 removal efficiencies were obtained from the magnetite/4,000 mg/L MLSS-AS hybrid process. The experiments showed that the RR195 removal from STW by M/AS increases with increasing MLSS and magnetite concentration concentrations. Higher RR195 removal efficiencies with higher biomass concentrations can be explained by

the increase of functional groups such as acidic polysaccharides, carboxyl, phosphonate, amino, hydroxyl groups, which are possibly responsible for the dye biosorption with increasing MLSS concentration [78]. Also, achieving higher removal efficiencies with higher magnetite concentrations is due to the presence of the more active binding sites [71]. The M/AS experiments showed that the optimum MLSS concentration is 4,000 mg/L to achieve sufficient dye removal efficiencies in shorter contact times and with lower magnetite concentrations. The experiments showed that the biosorption of RR195 by biomass and adsorption of RR195 by magnetite occurred in the M/AS process.

3.3.2. Effect of RR195 concentration on the removal of the RR195

Five different RR195 concentrations (50, 100, 150, 200, and 300 mg/L) were studied with the addition of different concentrations of the magnetite (1.25, 2.50, and 3.75 g/L) into the activated sludge containing 4,000 mg/L MLSS concentration (Fig. 8). The addition of 1.25 g/L magnetite into the 4,000 mg/L MLSS-AS was found to be sufficient for the removal of 50 mg/L RR195 with 99% efficiency within 45 min. 300 mg/L RR195 was removed with 77.8% efficiency within 90 min with 1.25 g/L magnetite/4,000 mg/L MLSS-AS. Removal efficiency of the 200 mg/L RR195 by 2.50 g/L magnetite/4,000 mg/L MLSS-AS within 120 min was calculated 99.50%. All RR195 concentrations were removed over 99% efficiency within different contact times by 3.75 g/L magnetite/4,000 mg/L MLSS-AS hybrid system.

3.3.3. COD removal from STW by M/AS process

The COD removal experiments were performed with 100 mg/L RR195 and different magnetite concentrations (1.25–5.0 g/L) in the activated sludge containing 2,000; 3,000 and 4,000 mg/L MLSS concentrations (Fig. 9). The COD removal efficiencies of M/AS and AS process were calculated for 120, 240, 360 and 1,440 min. The COD concentration of the STW was 2,155 mg·O_2/L. 85.25 mg·O_2/L of the total COD concentration is due to 100 mg/L RR195. The COD removal efficiencies increased with increasing magnetite concentration, time, and MLSS concentration. The COD removal efficiencies of 2,000; 3,000 and 4,000 mg/L MLSS-AS without magnetite within 2 h were found to be 73.45%, 78.58%, and 82.4%, respectively. The COD removal efficiencies for 4,000 mg/L MLSS-AS, 1.25 g/L magnetite/4,000 mg/L MLSS-AS, 5.0 g/L magnetite/4,000 mg/L MLSS-AS within 24 h were found to be 88.40%, 89.69%, and 94.32%, respectively. It was found that high amounts of magnetite and long contact times were required to remove the COD with >90% efficiency from STW. On the other hand, these requirements will change for textile wastewater containing lower COD values. After the M/AS treatment of STW, the magnetite particles were successfully

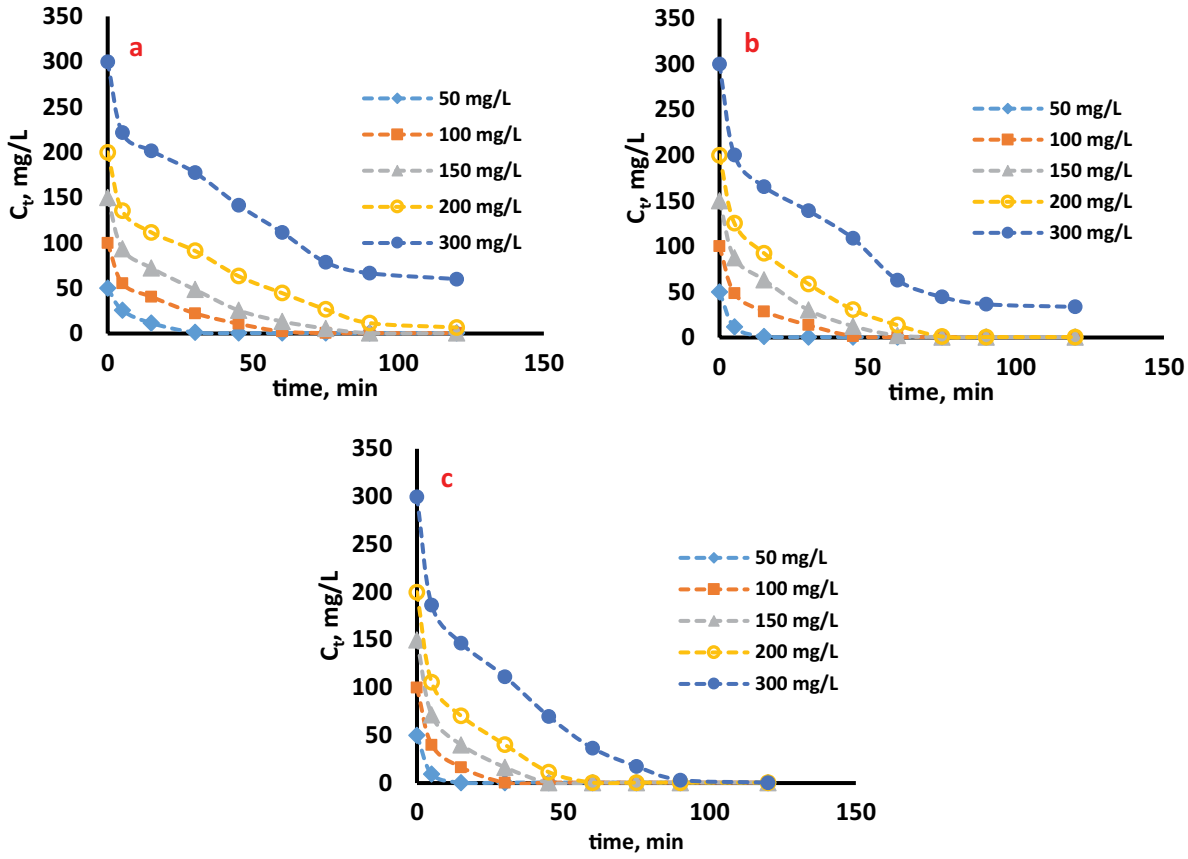

Fig. 8. Removal of different concentrations of the Reactive Red 195 by 1.25 g/L magnetite/4,000 MLSS-AS (a), 2.50 g/L magnetite/4,000 MLSS-AS (b), and 3.75 g/L magnetite/4,000 MLSS-AS (c).

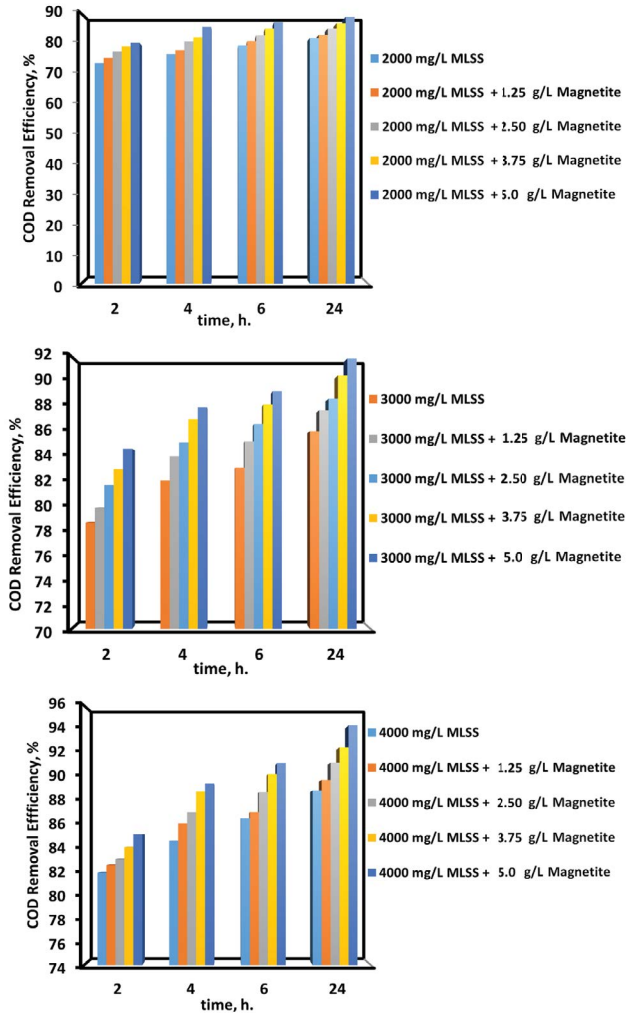

Fig. 9. Removal of the chemical oxygen demand by magnetite/activated sludge.

separated from the AS by application of external magnetic field (Fig. 10).

The studies on dye removal from wastewater generally focused on a single process such as adsorption or biological treatment [80–83]. In addition to dye molecules that are resistant to aerobic biodegradation, there are also biodegradable organic compounds in textile wastewater. While the adsorption process can be effective for the removal of dyes, it is not sufficient to reduce the COD concentration to the desired discharge levels. Aerobic biological processes such as AS generally show adequate performance in the mineralization of the biodegradable COD sources in textile wastewater. On the other hand, the AS process alone does not have sufficient performance in the removal of dye molecules in textile wastewater. Dye removal studies by live or dead AS biomass reported that the removal mechanism was biosorption not biodegradation [63,78,84]. Integration of adsorption and AS processes in a single reactor for the treatment of textile wastewater can provide advantages of these two processes. The fact that such an integrated hybrid system

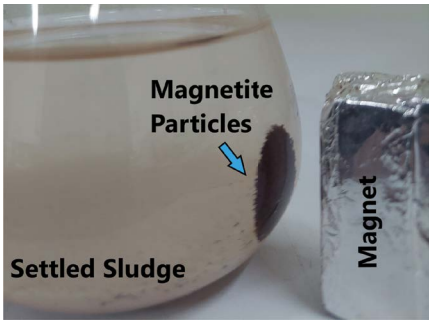

Fig. 10. Separation of the magnetite particles.

can be applied to AS processes by adding adsorbent provides significant convenience in practice. However, it is very important for sludge management that the adsorbent can be separated from the AS process after treatment. Addition of magnetite particles as an adsorbent to AS processes can be a potential hybrid process in the treatment of textile wastewater. However, no scientific research has been found on magnetic-adsorbent/AS integrated hybrid processes in the relevant literature. It is thought that this study is important in terms of filling the gap in the literature.

4. Conclusion

In the present study, the magnetite/activated sludge hybrid process (M/AS) was used for the removal of the RR195 from simulated textile wastewater. The Freundlich isotherm fits the experimental data obtained from the adsorption of RR195 by magnetite very well. The effect of MLSS and magnetite concentration on the removal of RR195 were investigated in M/AS process. The optimum MLSS concentration for removing the RR195 from STW by M/AS was determined as 4,000 mg/L. The RR195 removal efficiency within 90 min by 4,000 mg/L MLSS-AS and 2.5 g/L magnetite/4,000 mg/L MLSS-AS was found to be 76.10% and 99.50%, respectively. 94.32% COD removal efficiency was achieved by 5.0 g/L magnetite/4,000 mg/L MLSS-AS. The magnetite can be effectively separated from STW and biomass after M/AS treatment by an external magnetic field. M/AS is an eco-friendly adsorption/biodegradation hybrid process for the effective treatment of textile wastewater. The experiments have shown that the magnetite/AS hybrid process has a high potential in the treatment of dye-containing textile wastewater. Biosorption of RR195 and degradation of organic compounds by activated sludge and adsorption of RR195 by magnetite occur simultaneously in M/AS. The data obtained from the present study can be helpful in the treatment of textile wastewater by the adsorption/biodegradation hybrid process in real-scale applications. Magnetite can be easily separated from the AS by applying a magnetic field. Thus, inorganic load of biomass can be prevented during sludge treatment and disposal stages.

Disclosure statement

The authors declare that there are no conflicts of interest regarding the publication of this paper.

Acknowledgement

This study was financed by the Academic Research Projects Unit of the University of Cukurova, Project code FYL-2020-12438. The authors would like to thank to Cukurova University for their support.

References

[1] F.C.M. Tolentino, S.R. Sousa, C.D.Á.K. Cavalcanti, M.A. Granato, R.A.F. Machado, C. Marangoni, Membrane distillation for the recovery textile wastewater: influence of dye concentration, J. Water Process Eng., 46 (2022) 102611, doi: 10.1016/j.jwpe.2022.102611.

[2] L.T. Thao, T.V. Nguyen, V.Q. Nguyen, N.M. Phan, K.J. Kim, N.N. Huy, N.T. Dung, Orange G degradation by heterogeneous peroxymonosulfate activation based on magnetic $MnFe_2O_4$/α-MnO_2 hybrid, J. Environ. Sci., 124 (2023) 379–396.

[3] R. Al-Tohamy, S.S. Ali, F. Li, K.M. Okasha, Y.A.-G. Mahmoud, T. Elsamahy, H. Jiao, Y. Fu, J. Sun, A critical review on the treatment of dye-containing wastewater: ecotoxicological and health concerns of textile dyes and possible remediation approaches for environmental safety, Ecotoxicol. Environ. Saf., 231 (2022) 113160, doi: 10.1016/j.ecoenv.2021.113160.

[4] A. Albahnasawi, E. Yüksel, E. Gürbulak, F. Duyum, Fate of aromatic amines through decolorization of real textile wastewater under anoxic-aerobic membrane bioreactor, J. Environ. Chem. Eng., 8 (2020) 104226, doi: 10.1016/j.jece.2020.104226.

[5] R. Jamee, R. Siddique, Biodegradation of synthetic dyes of textile effluent by microorganisms: an environmentally and economically sustainable approach, Eur. J. Microbiol. Immunol., 9 (2019) 114–118.

[6] R. Rani, S. Tasmeem, A. Malik, V.K. Garg, L. Singh, S.B. Dhull, Optimization of Swiss blue dye removal by cotton boll activated carbon: response surface methodological approach, Toxin Rev., 41 (2022) 298–314.

[7] M.A. Ahmad, N.A.B. Ahmed, K.A. Adegoke, O.S. Bello, Adsorptive potentials of lemongrass leaf for methylene blue dye removal, Chem. Data Collect., 31 (2021) 100578, doi: 10.1016/j.cdc.2020.100578.

[8] M.A. Hassaan, A. El Nemr, F.F. Madkour, A.M. Idris, T.O. Said, T. Sahlabji, M.M. Alghamdi, A.A. El-Zahhar, Advanced oxidation of acid yellow 11 dye; detoxification and degradation mechanism, Toxin Rev., 40 (2021) 1472–1480.

[9] E.Y. Ozmen, M. Sezgin, A. Yilmaz, M. Yilmaz, Synthesis of β-cyclodextrin and starch based polymers for sorption of azo dyes from aqueous solutions, Bioresour. Technol., 99 (2008) 526–531.

[10] M. Paredes-Laverde, M. Salamanca, J.D. Diaz-Corrales, E. Flórez, J. Silva-Agredo, R.A Torres-Palma, Understanding the removal of an anionic dye in textile wastewaters by adsorption on $ZnCl_2$ activated carbons from rice and coffee husk wastes: a combined experimental and theoretical study, J. Environ. Chem. Eng., 9 (2021) 105685, doi: 10.1016/j.jece.2021.105685.

[11] S. Kalaiarasan, P. Uthirakumar, D.Y. Shin, I.H. Lee, The degradation profile of high molecular weight textile reactive dyes: a daylight induced photocatalytic activity of ZnO/carbon quantum dot photocatalyst, Environ. Nanotechnol. Monit. Manage., 15 (2021) 100423, doi: 10.1016/j.enmm.2020.100423.

[12] L. Ayed, N. Ladhari, R. El Mzoughi, K. Chaieb, Decolorization and phytotoxicity reduction of reactive blue 40 dye in real textile wastewater by active consortium: anaerobic/aerobic algal-bacterial-probiotic bioreactor, J. Microbiol. Methods, 181 (2021) 106129, doi: 10.1016/j.mimet.2020.106129.

[13] M. Suzuki, Y. Suzuki, K. Uzuka, Y. Kawase, Biological treatment of non-biodegradable azo-dye enhanced by zero-valent iron (ZVI) pre-treatment, Chemosphere, 259 (2020) 127470, doi: 10.1016/j.chemosphere.2020.127470.

[14] M. Haddad, S. Abid, M. Hamdi, H. Bouallagui, Reduction of adsorbed dyes content in the discharged sludge coming from an industrial textile wastewater treatment plant using aerobic activated sludge process, J. Environ. Manage., 223 (2018) 936–946.

[15] F. Cai, L. Lei, Y. Li, Y. Chen, A review of aerobic granular sludge (AGS) treating recalcitrant wastewater: refractory organics removal mechanism, application and prospect, Sci. Total Environ., 782 (2021) 146852, doi: 10.1016/j.scitotenv.2021.146852.

[16] L.J. Zhou, Z.Y. Rong, W. Gu, D.L. Fan, J.N. Liu, L.L. Shi, Y.H. Xu, Z.Y. Liu, Integrated fate assessment of aromatic amines in aerobic sewage treatment plants, Environ. Monit. Assess., 192 (2020) 1–14.

[17] M. Kozak, K. Cirik, S. Başak, Treatment of textile wastewater using combined anaerobic moving bed biofilm reactor and powdered activated carbon-aerobic membrane reactor, J. Environ. Chem. Eng., 9 (2021) 105596, doi: 10.1016/j.jece.2021.105596.

[18] N.D. Lourenço, R.D.G. Franca, M.A. Moreira, F.N. Gil, C.A. Viegas, H.M. Pinheiro, Comparing aerobic granular sludge and flocculent sequencing batch reactor technologies for textile wastewater treatment, Biochem. Eng. J., 104 (2015) 57–63.

[19] M. Jayapal, H. Jagadeesan, M. Shanmugam, S. Murugesan, Sequential anaerobic-aerobic treatment using plant microbe integrated system for degradation of azo dyes and their aromatic amines by-products, J. Hazard. Mater., 354 (2018) 231–243.

[20] B.E.L. Baeta, D.R.S. Lima, S.D.Q. Silva, S.F.D. Aquino, Evaluation of soluble microbial products and aromatic amines accumulation during a combined anaerobic/aerobic treatment of a model azo dye, Chem. Eng. J., 259 (2015) 936–944.

[21] H. Zhuang, J. Shi, S. Shan, L. Ping, C. Zhang, Enhanced anaerobic treatment of azo dye wastewater via direct interspecies electron transfer with Fe_3O_4/sludge carbon, Int. J. Hydrogen Energy, 45 (2020) 28476–28487.

[22] J. Liang, X.A. Ning, T. An, J. Sun, Y. Zhang, Y. Wang, Degradation of aromatic amines in textile-dyeing sludge by combining the ultrasound technique with potassium permanganate treatment, J. Hazard. Mater., 314 (2016) 1–10.

[23] Q. Liu, Y. Li, H. Chen, J. Lu, G. Yu, M. Möslang, Y. Zhou, Superior adsorption capacity of functionalised straw adsorbent for dyes and heavy-metal ions, J. Hazard. Mater., 382 (2020) 121040, doi: 10.1016/j.jhazmat.2019.121040.

[24] Y. Lin, Y. Dai, L. Zhang, Q. Wu, Efficient degradation of phenol in aqueous solution by $Fe^{2+}/H_2O_2/CaO_2$ system, Environ. Technol. Innovation, 27 (2022) 102320, doi: 10.1016/j.eti.2022.102320.

[25] L. García, J.C. Leyva-Díaz, E. Díaz, S. Ordóñez, A review of the adsorption-biological hybrid processes for the abatement of emerging pollutants: Removal efficiencies, physicochemical analysis, and economic evaluation, Sci. Total Environ., 780 (2021) 146554, doi: 10.1016/j.scitotenv.2021.146554.

[26] T. Widjaja, T. Miyata, Y. Nakano, W. Nishijima, M. Okada, Adsorption capacity of powdered activated carbon for 3,5-dichlorophenol in activated sludge, Chemosphere, 57 (2004) 1219–1224.

[27] R. Cao, S. Liu, X. Yang, C. Wang, Y. Wang, W. Wang, Y. Pi, Enhanced remediation of Cr(VI)-contaminated groundwater by coupling electrokinetics with ZVI/Fe_3O_4/AC-based permeable reactive barrier, J. Environ. Sci., 112 (2022) 280–290.

[28] Y. Xu, G. Wang, L. Zhu, W. Deng, C. Wang, T. Ren, b. Zhu, Z. Zeng, Desert beetle-like microstructures bridged by magnetic Fe_3O_4 grains for enhancing oil-in-water emulsion separation performance and solar-assisted recyclability of graphene oxide, Chem. Eng. J., 427 (2022) 130904, doi: 10.1016/j.cej.2021.130904.

[29] L. He, L. Wang, H. Zhu, Z. Wang, L. Zhang, L. Yang, Y. Dai, H. Mo, J. Zhang, J. Shen, A reusable Fe_3O_4/GO-COOH nanoadsorbent for Ca^{2+} and Cu^{2+} removal from oilfield wastewater, Chem. Eng. Res. Des., 166 (2021) 248–258.

[30] J. Chang, H. Wang, J. Zhang, Q. Xue, H. Chen, New insight into adsorption and reduction of hexavalent chromium by magnetite: multi-step reaction mechanism and kinetic model developing, Colloids Surf., A, 611 (2021) 125784, doi: 10.1016/j.colsurfa.2020.125784.

[31] M. Stan, I. Lung, M.L. Soran, O. Opris, C. Leostean, A. Popa, F. Copaciu, M.D. Lazar, I. Kacso, T.D. Silipas, A.S. Porav, Starch-coated green synthesized magnetite nanoparticles for removal of textile dye Optilan Blue from aqueous media, J. Taiwan Inst. Chem. Eng., 100 (2019) 65–73.
[32] M. Abu-Dalo, J. Abdelnabi, N.A. Al-Rawashdeh, B. Albiss, A. Al Bawab, Coupling coagulation-flocculation to volcanic tuff-magnetite nanoparticles adsorption for olive mill wastewater treatment, Environ. Nanotechnol. Monit. Manage., 17 (2022) 100626, doi: 10.1016/j.enmm.2021.100626.
[33] M.E. Mahmoud, M.F. Amira, M.M. Azab, A.M. Abdelfattah, An innovative amino-magnetite@graphene oxide@amino-manganese dioxide as a nitrogen-rich nanocomposite for removal of Congo red dye, Diamond Relat. Mater., 121 (2022) 108744, doi: 10.1016/j.diamond.2021.108744.
[34] M.A. Ali, M.F. Mubarak, M. Keshawy, M.A. Zayed, M. Ataalla, Adsorption of tartrazine anionic dye by novel fixed bed core-shell-polystyrene divinylbenzene/magnetite nanocomposite, Alexandria Eng. J., 61 (2022) 1335–1352.
[35] M.F. Khan, H. Ahmed, H.A. Almashhadani, M. Al-Bahrani, A.U. Khan, S. Ali, M. Zahid, Sustainable adsorptive removal of high concentration organic contaminants from water using biodegradable gum-acacia integrated magnetite nanoparticles hydrogel adsorbent, Inorg. Chem. Commun., 145 (2022) 110057, doi: 10.1016/j.inoche.2022.110057.
[36] A.O. Ezzat, A.M. Tawfeek, F. Mohammad, H.A. Al-Lohedan, Modification of magnetite nanoparticles surface with multifunctional ionic liquids for coomassie brilliant blue R-250 dye removal from aqueous solutions, J. Mol. Liq., 358 (2022) 119195, doi: 10.1016/j.molliq.2022.119195.
[37] A. Djafer, L. Djafer, B. Maimoun, A. Iddou, S. Kouadri Mostefai, A. Ayral, Reuse of waste activated sludge for textile dyeing wastewater treatment by biosorption: performance optimization and comparison, Water Environ. J., 31 (2017) 105–112.
[38] M.A. Aly-Eldeen, A.A. El-Sayed, D.M. Salem, G.M. El Zokm, The uptake of Eriochrome Black T dye from aqueous solutions utilizing waste activated sludge: adsorption process optimization using factorial design, Egypt. J. Aquat. Res., 44 (2018) 179–186.
[39] A. Kuleyin, A. Gök, F. Akbal, Treatment of textile industry wastewater by electro-Fenton process using graphite electrodes in batch and continuous mode, J. Environ. Chem. Eng., 9 (2021) 104782, doi: 10.1016/j.jece.2020.104782.
[40] H. Zhou, L. Zhou, K. Ma, Microfiber from textile dyeing and printing wastewater of a typical industrial park in China: occurrence, removal and release, Sci. Total Environ., 739 (2020) 140329, doi: 10.1016/j.scitotenv.2020.140329.
[41] M. Rahmayanti, Synthesis of magnetite nanoparticles using the reverse co-precipitation method with NH_4OH as precipitating agent and its stability test at various pH, Nat. Sci. J. Sci. Technol., 9 (2020) 54–58.
[42] Y.M. Zheng, H.Q. Yu, G.P. Sheng, Physical and chemical characteristics of granular activated sludge from a sequencing batch airlift reactor, Process Biochem., 40 (2005) 645–650.
[43] A.R.A. Aziz, P. Asaithambi, W.M.A.B.W. Daud, Combination of electrocoagulation with advanced oxidation processes for the treatment of distillery industrial effluent, Process Saf. Environ. Prot., 99 (2016) 227–235.
[44] X. Wang, J. Li, X. Zhang, Z. Chen, J. Shen, J. Kang, The performance of aerobic granular sludge for simulated swine wastewater treatment and the removal mechanism of tetracycline, J. Hazard. Mater., 408 (2021) 124762, doi: 10.1016/j.jhazmat.2020.124762.
[45] J. Wang, X. Guo, Adsorption isotherm models: classification, physical meaning, application and solving method, Chemosphere, 258 (2020) 127279, doi: 10.1016/j.chemosphere.2020.127279.
[46] P.S. Kumar, K. Ramakrishnan, S.D. Kirupha, S. Sivanesan, Thermodynamic and kinetic studies of cadmium adsorption from aqueous solution onto rice husk, Braz. J. Chem. Eng., 27 (2010) 347–355.
[47] E.E. Jasper, V.O. Ajibola, J.C. Onwuka, Nonlinear regression analysis of the sorption of crystal violet and methylene blue from aqueous solutions onto an agro-waste derived activated carbon, Appl. Water Sci., 10 (2020) 132, doi: 10.1007/s13201-020-01218-y.
[48] É.C. Lima, M.A. Adebayo, F.M. Machado, Kinetic and Equilibrium Models of Adsorption, C. Bergmann, F. Machado, Eds., Carbon Nanomaterials as Adsorbents for Environmental and Biological Applications, Carbon Nanostructures, Springer, Cham, 2015, pp. 33–69.
[49] M.A. Al-Ghouti, D.A. Da'ana, Guidelines for the use and interpretation of adsorption isotherm models: a review, J. Hazard. Mater., 393 (2020) 122383, doi: 10.1016/j.jhazmat.2020.122383.
[50] N. Ayawei, A.N. Ebelegi, D. Wankasi, Modelling and interpretation of adsorption isotherms, J. Chem., 2017 (2017) 3039817, doi: 10.1155/2017/3039817.
[51] I. Langmuir, Adsorption of gases on plain surfaces of glass mica platinum, J. Am. Chem. Soc., 40 (1918) 136–403.
[52] H.M. Freundlich, Over the adsorption in solution, J. Phys. Chem., 57 (1906) 385–470.
[53] V.S. Munagapati, H.Y. Wen, A.R. Gollakota, J.C. Wen, C.M. Shu, K.Y.A. Lin, Z. Tian, J.H. Wen, G.M. Reddy, G.V. Zyryanov, Magnetic Fe_3O_4 nanoparticles loaded papaya (*Carica papaya* L.) seed powder as an effective and recyclable adsorbent material for the separation of anionic azo dye (Congo red) from liquid phase: evaluation of adsorption properties, J. Mol. Liq., 345 (2022) 118255, doi: 10.1016/j.molliq.2021.118255.
[54] L.T. Popoola, Characterization and adsorptive behaviour of snail shell-rice husk (SS-RH) calcined particles (CPs) towards cationic dye, Heliyon, 5 (2019) e01153, doi: 10.1016/j.heliyon.2019.e01153.
[55] M.M. Majd, V. Kordzadeh-Kermani, V. Ghalandari, A. Askari, M. Sillanpää, Adsorption isotherm models: a comprehensive and systematic review (2010–2020), Sci. Total Environ., 812 (2021) 151334, doi: 10.1016/j.scitotenv.2021.151334.
[56] N. Taoufik, W. Boumya, R. Elmoubarki, A. Elhalil, M. Achak, M. Abdennouri, N. Barka, Experimental design, machine learning approaches for the optimization and modeling of caffeine adsorption, Mater. Today Chem., 23 (2022) 100732, doi: 10.1016/j.mtchem.2021.100732.
[57] R. Ramadoss, D. Subramaniam, Adsorption of chromium using blue green algae-modeling and application of various isotherms, Int. J. Chem. Technol., 10 (2018) 1–22.
[58] P.V.B. Leal, D.H. Pereira, R.M. Papini, Z.M. Magriotis, Effect of dimethyl sulfoxide intercalation into kaolinite on etheramine adsorption: experimental and theoretical investigation, J. Environ. Chem. Eng., 9 (2021) 105503, doi: 10.1016/j.jece.2021.105503.
[59] B. Zambrano Guisela, N. De Almeida Ohana, S. Duarte Dalvani, G. Velasco Fermin, H.M. Luzardo Francisco, N.-G. Luis, Adsorption of arsenic anions in water using modified lignocellulosic adsorbents, Results Eng., 13 (2022) 100340, doi: 10.1016/j.rineng.2022.100340.
[60] K. Nithya, A. Sathish, P.S. Kumar, T. Ramachandran, Fast kinetics and high adsorption capacity of green extract capped superparamagnetic iron oxide nanoparticles for the adsorption of Ni(II) ions, J. Ind. Eng. Chem., 59 (2018) 230–241.
[61] H. Montaseri, S. Alipour, M.A. Vakilinezhad, Development, evaluation and optimization of superparamagnetite nanoparticles prepared by co-precipitation method, Res. Pharm. Sci., 12 (2017) 274–282.
[62] S.K. Panda, I. Aggarwal, H. Kumar, L. Prasad, A. Kumar, A. Sharma, D.V.N. Vo, D.V. Thuan, V. Mishra, Magnetite nanoparticles as sorbents for dye removal: a review, Environ. Chem. Lett., 19 (2021) 2487–2525.
[63] M. Masuku, L. Ouma, A. Pholosi, Microwave assisted synthesis of oleic acid modified magnetite nanoparticles for benzene adsorption, Environ. Nanotechnol. Monit. Manage., 15 (2021) 100429, doi: 10.1016/j.enmm.2021.100429.
[64] W.-H. Lee, J.-O. Kim, Phosphate recovery from anaerobic digestion effluent using synthetic magnetite particles,

J. Environ. Chem. Eng., 10 (2021) 107103, doi: 10.1016/j.jece.2021.107103.
[65] S. Khorshidi, A. Karkhaneh, S. Bonakdar, Fabrication of amine-decorated nonspherical microparticles with calcium peroxide cargo for controlled release of oxygen, J. Biomed. Mater. Res. Part A, 108 (2020) 136–147.
[66] S.V. Gopal, I.H. Joe, Bio-activity of superparamagnetic maghemite nanorods capped with DL-alanine, J. Mol. Liq., 234 (2017) 382–390.
[67] V. Harnchana, A. Phuwongkrai, C. Thomas, V. Amornkitbamrung, Facile and economical synthesis of superparamagnetic magnetite nanoparticles coated with oleic acid using sonochemical route, Mater. Today Proc., 5 (2018) 13995–14001.
[68] N. Jude, F. Josepha, T.N. Derek, M.Y. Divine, W.M.K. Rui, Synthesis and magnetic properties of a superparamagnetic nanocomposite "pectin-magnetite nanocomposite", J. Nanomater., 2013 (2013) 137275, doi: 10.1155/2013/137275.
[69] S.S. Gupta, K.G. Bhattacharyya, Kinetics of adsorption of metal ions on inorganic materials: a review, Adv. Colloid Interface Sci., 162 (2011) 39–58.
[70] F. Akbal, Adsorption of basic dyes from aqueous solution onto pumice powder, J. Colloid Interface Sci., 286 (2005) 455–458.
[71] T.A. Aragaw, A.N. Alene, A comparative study of acidic, basic, and reactive dyes adsorption from aqueous solution onto kaolin adsorbent: effect of operating parameters, isotherms, kinetics, and thermodynamics, Emerging Contam., 8 (2022) 59–74.
[72] K. Rybka, J. Matusik, M. Marzec, Mg/Al and Mg/Fe layered double hydroxides derived from magnesite and chemicals: the effect of adsorbent features and anions chemistry on their removal efficiency, J. Cleaner Prod., 332 (2022) 130084, doi: 10.1016/j.jclepro.2021.130084.
[73] M. Mesbah, S. Hamedshahraki, S. Ahmadi, M. Sharifi, C.A. Igwegbe, Hydrothermal synthesis of $LaFeO_3$ nanoparticles adsorbent: characterization and application of error functions for adsorption of fluoride, MethodsX, 7 (2020) 100786, doi: 10.1016/j.mex.2020.100786.
[74] F. Barjasteh-Askari, M. Davoudi, M. Dolatabadi, S. Ahmadzadeh, Iron-modified activated carbon derived from agro-waste for enhanced dye removal from aqueous solutions, Heliyon, 7 (2021) e07191, doi: 10.1016/j.heliyon.2021.e07191.
[75] J.F. Gao, Q. Zhang, J.H. Wang, X.L. Wu, S.Y. Wang, Y.Z. Peng, Contributions of functional groups and extracellular polymeric substances on the biosorption of dyes by aerobic granules, Bioresour. Technol., 102 (2011) 805–813.
[76] N. Caner, I. Kiran, S. Ilhan, C.F. Iscen, Isotherm and kinetic studies of Burazol Blue ED dye biosorption by dried anaerobic sludge, J. Hazard. Mater., 165 (2009) 279–284.
[77] O. Gulnaz, A. Kaya, S. Dincer, The reuse of dried activated sludge for adsorption of reactive dye, J. Hazard. Mater., 134 (2006) 190–196.
[78] Z. Aksu, A.B. Akın, Comparison of Remazol Black B biosorptive properties of live and treated activated sludge, Chem. Eng. J., 165 (2010) 184–193.
[79] J. Cai, L. Cui, Y. Wang, C. Liu, Effect of functional groups on sludge for biosorption of reactive dyes, J. Environ. Sci., 21 (2009) 534–538.
[80] C. Hao, G. Li, G. Wang, W. Chen, S. Wang, Preparation of acrylic acid modified alkalized MXene adsorbent and study on its dye adsorption performance, Colloids Surf., A, 632 (2022) 127730, doi: 10.1016/j.colsurfa.2021.127730.
[81] T. Patra, A. Mohanty, L. Singh, S. Muduli, P.K. Parhi, T.R. Sahoo, Effect of calcination temperature on morphology and phase transformation of MnO_2 nanoparticles: a step towards green synthesis for reactive dye adsorption, Chemosphere, 288 (2022) 132472, doi: 10.1016/j.chemosphere.2021.132472.
[82] A.H. Birniwa, H.N.M.E. Mahmud, S.S.A. Abdullahi, S. Habibu, A.H. Jagaba, M.N.M. Ibrahim, A. Ahmad, M.B. Alshammari, T. Parveen, K. Umar, Adsorption behavior of methylene blue cationic dye in aqueous solution using polypyrrole-polyethylenimine nano-adsorbent, Polymers, 14 (2022) 3362, doi: 10.3390/polym14163362.
[83] R. Gajera, R.V. Patel, A. Yadav, P.K. Labhasetwar, Adsorption of cationic and anionic dyes on photocatalytic flyash/TiO_2 modified chitosan biopolymer composite, J. Water Process. Eng., 49 (2022) 102993, doi: 10.1016/j.jwpe.2022.102993.
[84] A. Berrazoum, R. Marouf, F. Ouadjenia, J. Schott, Bioadsorption of a reactive dye from aqueous solution by municipal solid waste, Biotechnol. Rep., 7 (2015) 44–50.